Paper Number:

Title: **A stabilized finite element method for modeling mixed-mode delamination of composites**

Authors: Gourab Ghosh[1]

Chandrasekhar Annavarapu [2]

Stephen Jiménez[1]

Ravindra Duddu[1]

---

[1]Department of Civil and Environmental Engineering, Vanderbilt University, Nashville, Tennessee.

[2]Atmospheric, Earth, and Energy Division, Lawrence Livermore National Laboratory, Livermore, California.

ABSTRACT

Delamination of composite materials is commonly modeled using intrinsic cohesive zone models (CZMs), which are generally incorporated into the standard finite element (FE) method through a zero-thickness interface (cohesive) element; however, intrinsic CZMs exhibit numerical instabilities when the cohesive stiffness parameters is assumed to be large relative to the elastic stiffness of the composite material. To address this numerical instability issue, we propose a stabilized finite element method by combining the traditional penalty method with the Nitsche's method that is equally effective for any specified initial stiffness of the cohesive (traction-separation) law. The key advantage of the proposed method is that it generalizes the Nitsche's method to any traction-separation law with arbitrary large values of initial stiffness and provides a unified way to treat cohesive fracture problems in a variationally consistent and stable manner. We implemented the stabilized method in the commercial finite element software Abaqus via the user element subroutine and simulated benchmark tests for mode I and mixed-mode delamination in isotropic materials to establish the viability of the approach. Ongoing work is aimed at extending the method to model delamination in transversely isotropic laminated composites.

INTRODUCTION

Cohesive zone models (CZMs) were first proposed by [1],[2] and are widely used for modeling fracture and fatigue crack growth. The key advantages of CZMs are that they do not require the presence of a initial (or pre-existing) crack and account for the finite size of the fracture process zone (FPZ) at the crack tip, unlike the linear elastic fracture mechanics approaches. Therefore, CZMs are suited for modeling delamination of composite materials, where the FPZ may be greater than the characteristic length scales. One of the ways to implement cohesive zone models in the finite element (FE) framework is using zero-thickness interface elements, wherein the interface (or cohesive) elements are placed along the probable crack path and their constitutive (traction-separation) behavior is defined by so-called "cohesive laws". There are two classes of cohesive laws, namely intrinsic traction-separation laws or initially elastic cohesive laws, and extrinsic traction-separation laws or initially rigid cohesive laws (see Figure 1). The major difference between the intrinsic and the extrinsic traction separation laws is the presence of the initial elastic curve [3]. In the case of intrinsic laws, the traction is assumed to gradually increase with the separation and after reaching a maximum value, it decreases monotonically till the separation reaches the ultimate separation value (i.e., where complete de-cohesion is assumed to occur). Whereas, in extrinsic laws, it is assumed that only after traction reaches a finite cohesive strength, the separation starts and the traction decreases monotonically with the increase in separation.

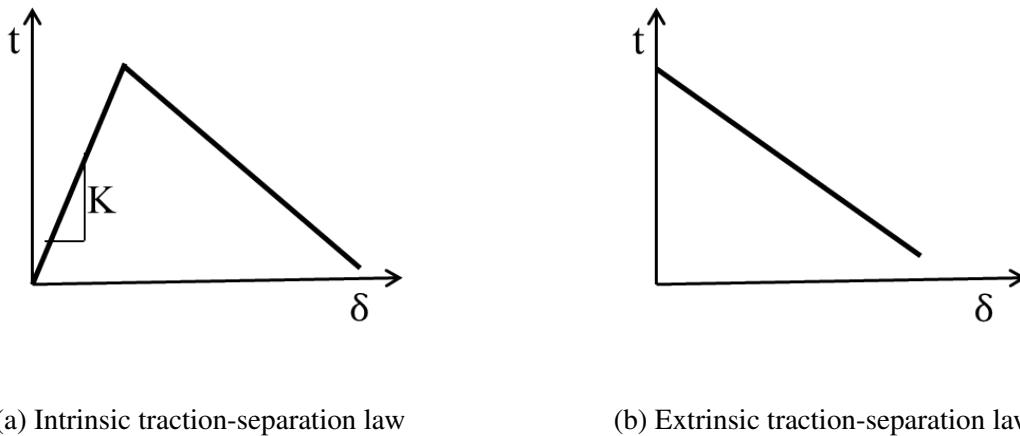(a) Intrinsic traction-separation law   (b) Extrinsic traction-separation law

Figure 1: Intrinsic and extrinsic traction separation laws

The numerical implementation of extrinsic traction separation law is challenging [4] because advanced data structures are required to store the finite element discretization. Furthermore, parallelization of finite element codes in conjugation with extrinsic laws is not a trivial task due to the

change of the mesh topology with the advancement of cracks. Although researchers have proposed several ways (e.g., topology-based data structures [5]; scalable parallel implementation [6]) to alleviate the above-mentioned challenges, the complexities in its implementation are key deterrent for its widespread use. Intrinsic cohesive laws, on the other hand are easier to implement in a FE code; however, they suffer from the artificial compliance [7] due to elasticity of the cohesive law. This issue can be solved to some extent by restricting the time step to an extremely small value [8], but this may result in an impractically high computation cost. Another approach to solve this problem is to use very high initial elastic slope for the intrinsic law [7], but that causes an ill-conditioning of the tangent stiffness matrices. Thus, following a conventional approach to treat above-mentioned problems within a finite element framework poses numerical challenges, and has motivated researchers to come up with novel approaches to overcome the disadvantages posed by the intrinsic traction-separation laws. For example, a hybrid discontinuous Galerkin (dG) and extrinsic traction-separation law was proposed by [9]; in this approach, interface elements are inserted between bulk elements at the beginning of the analysis and continuity during the elastic regime is maintained in a weak manner by a dG formulation, but upon onset of failure the extrinsic traction separation law replaces the dG formulation. However, it has been recognized [4] that implementing extrinsic traction-separation law in conjunction with dG method in commercial software (e.g., Abaqus) is extremely difficult. Thus, this hybrid approach is effective in overcoming some disadvantages of the intrinsic CZMs, but it is not easy to implement them in commercial codes.

Directed at achieving the same goal of removing the artificial compliance issue associated with the intrinsic laws, a continuum approach was proposed by [10]. Two of the major types of the continuum approaches for enforcing continuity weakly at the interface are: Lagrange multiplier methods and discontinuous Galerkin (dG) methods. The work of [10] was motivated by an augmented Lagrange multiplier-based mixed interface element approach proposed by [11]. In Lagrange multiplier method, it is challenging to construct a stable Lagrange multiplier space. It has been shown by [12] that for embedded finite element methods it is difficult to find a stable Lagrange multiplier. A stable choice of Lagrange multipliers is important from the standpoint of removing artificial oscillations in the interfacial traction. The second key alternative, that is, dG method originated from the Nitsche's method [13]. The Nitsche's method can be seen as a variationally consistent penalty method. In the penalty method (introduced in [14]), Dirichlet constraint at the interface is enforced by introducing a spring at the interface, and a better approximation for the Dirichlet constraint can be obtained with an increase in penalty parameter (i.e., the stiffness of the spring/ slope of the traction separation law). The interfacial constraints are achieved exactly when the stiffness approaches to infinity, but this implies that the method is variationally inconsistent. Also, a very high value of stiffness results in an ill-conditioned system of equations. Whereas, Nitsche's method not only eliminates the instability issues (evident from [15]) related with the standard penalty methods by adding consistency terms ([16]), but also yields a well-conditioned system of discrete equations if the method parameters are chosen appropriately. This method has been used for solving a wide class of interface problems in an efficient way ([17], [18]). A comprehensive review of the classical Nitsche's method and it's application to interface problems can be found in [19]. Recently a precise definition of the weights and a closed form analytical expression of the stabilization parameter was proposed by [18]; this weighted Nitsche method provides much

accurate results in comparison to the standard Nitsche method. Thus, it is evident that although the Nitsche's method-based consistent penalty and dG approaches are well established for treating embedded interface problems, relatively little work has been done in extending these methods to generalized intrinsic cohesive laws.

In this article, we will discuss a stabilized finite element method for alleviating the artificial compliance issue inherent to the intrinsic cohesive law with very high value of cohesive stiffness. The key advantage of the proposed method is that it generalizes the Nitsche's method to any traction-separation law with arbitrary large values of initial stiffness and provides a unified way to treat cohesive fracture problems in a variationally consistent and stable manner. The rest of this article is organized as follows: in the Section , we introduce the model problem and the associated variational formulation. In section 3, we discuss the spatial discretization followed by numerical examples demonstrating the accuracy and efficacy of the approach in Section 4. Finally, the last section provides a summary and some concluding remarks.

MODEL PROBLEM AND VARIATIONAL FORMULATION

In this section, we present details of the stabilized Nitsche formulation for treating general cohesive laws. We first explain the notation for variables and the problem domain, followed by a discussion of the strong form and the weak form of the governing equations for linear elastostatics and cohesive fracture. We present the model equations in indicial notation with Einstein's summation convention and reserve the right superscript for exponents (italicized) or descriptors (unitalicized).

Domain Description

We define a domain $\Omega \subset \mathbb{R}^2$, which is partitioned into two non-overlapping bulk domains Ω^m (where m=1,2 and $\Omega = \Omega^1 \cup \Omega^2$) separated by an embedded crack surface Γ_* (Fig. 2). Both the bulk domains consist of homogeneous, linear, isotropic, and elastic material. Dirichlet and Neumann boundary conditions are defined on the parts of the domain boundary ($\Gamma \equiv \partial\Omega$) excluding the embedded interface boundary (Γ_*). The parts of the boundary where Dirichlet and Neumann conditions are defined are denoted as Γ_d^m and Γ_n^m, respectively. The unit normal to the boundary of each subdomain, $\mathbf{n}^m$, points outwards from the domain Ω^m.
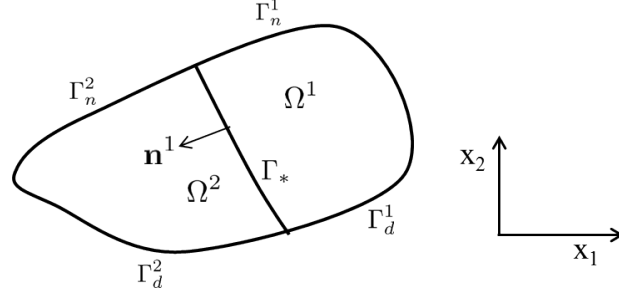
Figure 2: Domains Ω^1 and Ω^2 separated by a shared boundary Γ_*. The Dirichlet boundaries (Γ_d^1, Γ_d^2) and the Neumann boundaries (Γ_n^1, Γ_n^2) are as shown. The complementary part of the boundary is traction free. The normal to the boundary of each subdomain, $\mathbf{n}^m$, points outwards from the domain Ω^m as shown

Strong Form

The governing equations of equilibrium without body force in each of the domains are given by:

$$\sigma_{ij,j}^m = 0 \ \text{in} \ \Omega^m, \tag{1}$$

$$u_i^m = \bar{u}_i^m \ \text{on} \ \Gamma_d^m, \tag{2}$$

$$\sigma_{ij}^m n_j^m = h_i^m \ \text{on} \ \Gamma_n^m, \tag{3}$$

where σ_{ij}^m and u_i^m denote the components of the stress and displacement fields in the domain Ω^m, respectively, and n_j^m denotes the components of the unit outward normal. On the Dirichlet portion of the boundary, the displacement is fixed to the prescribed field $\bar{u}_i^m$ and on the Neumann portion of the boundary, prescribed traction is denoted by h_i^m. The traction field t_i^m on the embedded crack interface can be obtained by projecting the stress from each domain and is related to the interface separation $[\![u_i]\!] = u_i^2 - u_i^1$ according to an assumed traction-separation law, that is,

$$t_i^m = \sigma_{ij}^m n_j^m = f([\![u_i]\!]) \ \text{on} \ \Gamma_*, \tag{4}$$

To represent the mode I and mode II cohesive fracture behavior in two dimensions, we use the normal and tangential coordinate system $(\mathbf{n}^m, \boldsymbol{\tau}^m)$. Accordingly, the tangential (t_τ) and normal (t_n) components of the traction vector are defined by:

$$t_i^m = t_n n_i^m + t_\tau \tau_i^m, \tag{5}$$

$$u_i^m = u_n n_i^m + u_\tau \tau_i^m, \tag{6}$$

$$t_n = -\alpha_n [\![u_n]\!], \tag{7}$$

$$t_\tau = -\alpha_\tau [\![u_\tau]\!], \tag{8}$$

where α_n and α_τ represents the cohesive stiffness in the normal and the tangential direction, respectively. The force balance on the interface is given by:

$$t_i^1 + t_i^2 = 0 \ \text{on} \ \Gamma_*. \tag{9}$$

Equations (7) and (8) can used to represent general cohesive laws by using the damage mechanics framework described in [20, 21, 22, 23]; herein, we consider a bilinear intrinsic traction separation law. The constitutive equations for the linear, elastic, isotropic bulk domains are given by:

$$\sigma_{ij}^m = C_{ijkl}^m \varepsilon_{kl}^m = C_{ijkl}^m u_{(k,l)}^m \ \text{ in } \ \Omega^m, \tag{10}$$

where C_{ijkl}^m, ε_{kl}^m and $u_{(k,l)}^m$ denote the fourth-order elasticity tensor, the second-order strain tensor, and the symmetric gradient of the displacement field, respectively.

Weak Form

In this section, we follow the weighted residual approach [18] and define the solution spaces $\mathbb{U} = \mathbb{U}^1 \times \mathbb{U}^2$ and trial spaces $\mathbb{W} = \mathbb{W}^1 \times \mathbb{W}^2$ respectively, such that:

$$\mathbb{U}^m = \{u^m \in H^1(\Omega^m), u^m = \bar{u}_i^m \ \text{ on } \ \Gamma_d^m\}, \tag{11}$$
$$\mathbb{W}^m = \{w^m \in H^1(\Omega^m), w^m = 0 \ \text{ on } \ \Gamma_d^m\}. \tag{12}$$

Following the standard finite element approach, we get

$$\int_\Omega w_{(i,j)}^m \sigma_{ij}^m d\Omega - \sum_m \int_{\Gamma_*} (w_n^m t_n^m + w_\tau^m t_\tau^m) d\Gamma = \int_{\Gamma_n} w_i^m h_i^m d\Gamma. \tag{13}$$

By substituting expressions for t_n and t_τ from Equations (7) and (8) in the above equation, we get

$$\int_\Omega w_{(i,j)}^m \sigma_{ij}^m d\Omega + \int_{\Gamma_*} (\llbracket w_n \rrbracket \alpha_n \llbracket u_n \rrbracket + \llbracket w_\tau \rrbracket \alpha_\tau \llbracket u_\tau \rrbracket) d\Gamma = \int_{\Gamma_n} w_i^m h_i^m d\Gamma. \tag{14}$$

Equation (14) is the standard weak form for the penalty method. It is evident that as $\alpha_n \to \infty$ and $\alpha_\tau \to \infty$, solving Equation (14) is an ill-posed problem. To alleviate the ill-posedness of the weak form, we adopt a Nitsche's method-based stabilized FE approach. We begin by re-scaling the normal and tangential traction components and followed by some algebraic manipulations arrive at the final stabilized weak form as given by

$$\int_\Omega w_{(i,j)} \sigma_{ij} d\Omega - \int_{\Gamma_*} \left(\left(\frac{\alpha_n}{\alpha_n + \beta_n} \right) \llbracket w_n \rrbracket p_\gamma + \left(\frac{\alpha_\tau}{\alpha_\tau + \beta_\tau} \right) \llbracket w_\tau \rrbracket f_\gamma \right) d\Gamma$$
$$+ \int_{\Gamma_*} \left(\frac{\alpha_n \beta_n}{\alpha_n + \beta_n} \llbracket w_n \rrbracket \llbracket u_n \rrbracket + \frac{\alpha_\tau \beta_\tau}{\alpha_\tau + \beta_\tau} \llbracket w_\tau \rrbracket \llbracket u_\tau \rrbracket \right) d\Gamma = \int_{\Gamma_n} w_i h_i d\Gamma, \tag{15}$$

where p_γ and f_γ are the weighted interfacial pressure and shear, respectively, as defined by

$$p_\gamma = n_j^2 < \sigma_{ij} >_\gamma n_j^2 \ ; \ f_\gamma = \tau_j^2 < \sigma_{ij} >_\gamma n_j^2; \tag{16}$$

and $< \sigma_{ij} >_\gamma = \gamma^1 \sigma_{ij}^1 + \gamma^2 \sigma_{ij}^2$ represents a weighted average of stress across the interface. The weights γ^1 and γ^2 are positive and satisfy the condition $\gamma^1 + \gamma^2 = 1$. Note that Equation (15) is well-defined even as α_n or $\alpha_\tau \to \infty$. On the other hand, if β_n and $\beta_\tau \to \infty$, we get a standard penalty weak-form defined in Equation (14).

SPATIAL DISCRETIZATION

We discretized the domain Ω into bilinear plane strain quadrilateral bulk or continuum elements and introduce zero-thickness cohesive elements at the interface boundary. The approximated displacement field is defined as

$$\mathbf{u}^m = \mathbf{N}^m \mathbf{a}^m, \quad m = 1, 2, \tag{17}$$

where $\mathbf{N}^m$ is the element shape function matrix and $\mathbf{a}^m$ denotes the element vector containing the displacement degrees of freedom (DOFs). The displacement jump at the interface $[\![\mathbf{u}]\!]$ is given by

$$[\![\mathbf{u}]\!] = \mathbf{u}^1 - \mathbf{u}^2 = \mathbf{N}^1 \mathbf{a}^1 - \mathbf{N}^2 \mathbf{a}^2, \tag{18}$$

where $\mathbf{a}^m$ (m=1,2) denotes the nodal displacement vector of the continuum subdomain Ω^m (m=1,2) adjacent to Γ_*. The shape function matrix $\mathbf{N}^m$ can be represented as

$$\mathbf{N}^m = \begin{bmatrix} N_1^m & 0 & N_2^m & 0 & N_3^m & 0 & N_4^m & 0 \\ 0 & N_1^m & 0 & N_2^m & 0 & N_3^m & 0 & N_4^m \end{bmatrix}, \tag{19}$$

where N_J^m ($J = 1, 2, 3, 4$) are the shape functions of four-noded quadrilateral bulk elements. After we introduce the discretized form for the approximation spaces into the variational form in Equation (13), it leads us to the following discrete equation of equilibrium in the residual form

$$\mathbf{R}(\mathbf{u}) = \mathbf{f}_{\text{ext}} - (\mathbf{f}_{\text{int}}^b + \mathbf{f}_{\text{int}}^c). \tag{20}$$

Note that the residual vector contributes to the RHS term in the Abaqus UEL subroutine. Neglecting body forces, $\mathbf{f}_{\text{ext}}$ is obtained by assembling the element contributions from traction boundary conditions on the Neumann boundary

$$\mathbf{f}_{\text{ext}} = \sum_e \int_{\Gamma_{ne}^m} \mathbf{N}^{mT} \mathbf{h}^m \, d\Gamma_e \quad \text{for m=1,2.} \tag{21}$$

where $\sum_e$ indicates the matrix (or vector) assembly of the global system from the element matrices (or vectors) in entire computational domain. The internal bulk force vector $\mathbf{f}^b_{int}$ is assembled as

$$\mathbf{f}^b_{int} = \sum_e \int_{\Omega^m_e} \mathbf{B}^{mT} \mathbf{C}^m \mathbf{B}^m \mathbf{u}^m_e \, d\Omega_e \text{ for m=1,2,} \tag{22}$$

where $\mathbf{B}^m$ is the strain-displacement relationship matrix, and $\mathbf{C}^m$ is the elasticity matrix in Voigt notation. The strain-displacement relationship matrix is given by

$$\mathbf{B}^m = \begin{bmatrix} N^m_{1,1} & 0 & N^m_{2,1} & 0 & N^m_{3,1} & 0 & N^m_{4,1} & 0 \\ 0 & N^m_{1,2} & 0 & N^m_{2,2} & 0 & N^m_{3,2} & 0 & N^m_{4,2} \\ N^m_{1,2} & N^m_{1,1} & N^m_{2,2} & N^m_{2,1} & N^m_{3,2} & N^m_{3,1} & N^m_{4,2} & N^m_{4,1} \end{bmatrix}, \tag{23}$$

where $N^m_{J,1}$ denotes the derivative of the shape function N^m_J with respect to x_1 in Ω^m. The cohesive element contribution to the internal force vector $\mathbf{f}^c_{int}$ is assembled as

$$\mathbf{f}^c_{int} = \mathbf{f}^{stabilized} + \mathbf{f}^{consistency} = \int_{\Gamma_{*e}} \mathbf{N}^T \mathbf{S} \mathbf{t} \, d\Gamma_e + \int_{\Gamma_{*e}} \mathbf{N}^T (\mathbf{I} - \mathbf{S}) \mathbf{T} \boldsymbol{\sigma}_\gamma \, d\Gamma_e \tag{24}$$

where $\mathbf{S}$ is the 2×2 stabilization matrix, $\mathbf{I}$ is the 2×2 identity matrix, $\mathbf{t} = [t_\tau, t_n]^T$ is the cohesive traction vector that is a function of the displacement jump vector $[\![\mathbf{u}]\!]$, $\mathbf{T}$ is the stress transformation matrix and $\boldsymbol{\sigma}_\gamma$ is the weighted stress vector in Voigt notation for in-plane stress components.

Let us now define the element tangent matrix $\mathbf{K}$ that contributes to the AMATRX term in the Abaqus UEL subroutine. The element tangent matrix is obtained by assembling the contributions of the bulk and cohesive tangent matrices, that is,

$$\mathbf{K} = -\frac{\partial \mathbf{R}}{\partial \mathbf{u}} = \frac{\partial \mathbf{f}^b_{int}}{\partial \mathbf{u}} + \frac{\partial \mathbf{f}^c_{int}}{\partial \mathbf{u}} = \mathbf{K}^b + \mathbf{K}^c, \tag{25}$$

where,

$$\mathbf{K}^b = \sum_e \int_{\Omega^m_e} \mathbf{B}^T \mathbf{C}^m \mathbf{B} \, d\Omega_e \text{ for m=1,2} \tag{26}$$

and

$$\mathbf{K}^c = \mathbf{K}^{stabilized} + \mathbf{K}^{consistency} = \sum_e \int_{\Gamma_{*e}} [\![\mathbf{N}]\!]^T \mathbf{S} \mathbf{M} [\![\mathbf{N}]\!] \, d\Gamma_e + \sum_e \int_{\Gamma_{*e}} [\![\mathbf{N}]\!]^T (\mathbf{I} - \mathbf{S}) \mathbf{T} \mathbf{C} \mathbf{B}_\gamma \, d\Gamma_e. \tag{27}$$

In the above equation: the jump in shape function matrix $[\![\mathbf{N}]\!]$ is represented as follows

$$[\![\mathbf{N}]\!] = \begin{bmatrix} -N^1 & 0 & -N^2 & 0 & N^2 & 0 & N^1 & 0 \\ 0 & -N^1 & 0 & -N^2 & 0 & N^2 & 0 & N^1 \end{bmatrix}, \tag{28}$$

where N^m (m=1,2) represents the linear shape functions evaluated at the interface Gauss points

(GPs); the weighted shape function gradient matrix $\mathbf{B}_\gamma$ is given by

$$\mathbf{B}_\gamma = \begin{bmatrix} \gamma\mathbf{B}^+ & (1-\gamma)\mathbf{B}^- \end{bmatrix}, \tag{29}$$

where $\mathbf{B}^+$ and $\mathbf{B}^-$ are matrices containing gradient of the shape functions calculated at the interface GPs from the neighboring bulk domains of the cohesive element; the stress transformation matrix $\mathbf{T}$ is defined as

$$\mathbf{T} = \begin{bmatrix} -CS & CS & C^2 - S^2 \\ S^2 & C^2 & -2CS \end{bmatrix}, \tag{30}$$

where C and S represent $\cos\theta$ and $\sin\theta$, respectively, and θ is the inclination of the cohesive element with the x_1 coordinate direction; the cohesive stiffness matrix $\mathbf{M}$ and the stabilization matrix $\mathbf{S}$ are defined as

$$\mathbf{M} = \begin{bmatrix} \frac{\partial t_\tau}{\partial u_\tau} & \frac{\partial t_\tau}{\partial u_n} \\ \frac{\partial t_n}{\partial u_\tau} & \frac{\partial t_n}{\partial u_n} \end{bmatrix}; \quad \mathbf{S} = \begin{bmatrix} \frac{\beta_t}{M_{11}+\beta_t} & \frac{\beta_t}{M_{12}+\beta_t} \\ \frac{\beta_n}{M_{21}+\beta_n} & \frac{\beta_n}{M_{22}+\beta_n} \end{bmatrix}. \tag{31}$$

Figure 3 gives an overview of the implementation of the proposed approach in commercial FE software Abaqus. The presence of weighted average of stress and shape function derivatives across the interface implies that the computation of cohesive element tangent matrices and the residual vectors depends on the displacement shape functions associated with their nodes as well as those in the two neighboring bulk elements. In our scheme, we calculate these quantities at the interface GPs in the UELMAT subroutine for the bulk elements, and then pass them to the UEL subroutine for the cohesive elements using global modules. These set of calculations are done separate from the standard loop over bulk GPs for assembling the bulk stiffness matrix and right hand side (RHS) vector. The element tangent matrix is unsymmetric and $\mathbf{K}^{\text{consistency}}$ has the dimension of 8×16 (the number of rows correspond to the interfacial degrees of freedoms (DoFs) and the number of columns correspond to the interfacial and adjacent bulk element DoFs) for the setup (Fig. 4). As a cohesive interface element has only four nodes associated with it and two DoFs defined at each of them, it can only assemble a stiffness matrix of size 8×8. To resolve this implementation issue, we use "dummy" elements (elements IV-VII in Fig. 4) in the UEL subroutine that facilitate the partition and assembly of the stiffness matrix in Abaqus.

NUMERICAL EXAMPLES

In this section, we first verify the proposed stabilized finite element formulation, by performing uniaxial tension test and comparing numerically obtained solution with the analytical solution. Next, we simulate mode I and mixed mode bending tests using the proposed methodology to demonstrate the its applicability to large scale complex problems. All simulations are performed in two dimensions assuming plane strain conditions. We assume linear, elastic, and isotropic material
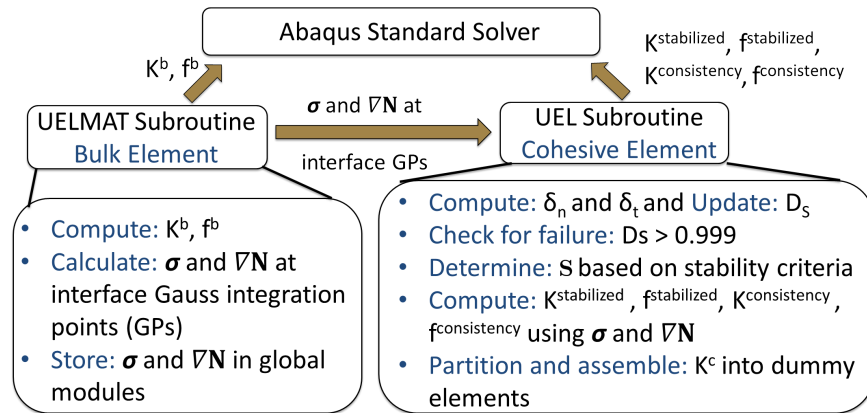
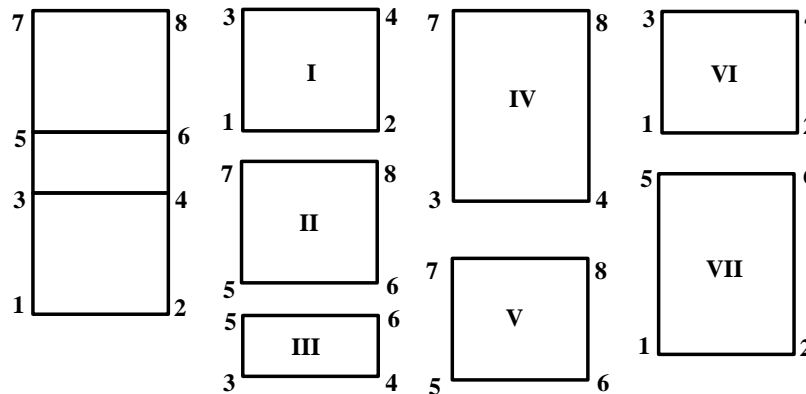Figure 3: Abaqus flowchart showing interaction between UELMAT and UEL

Figure 4: Bulk (I and II), cohesive (III), and dummy (IV-VII) elements

behavior for the simulations. Table I shows a summary of the material properties considered for each of the test cases.

Uniaxial Tension Test

To perform the uniaxial tension test, a vertical displacement (δ) is applied at the upper two nodes (i.e., nodes 7 and 8) of the model (leftmost diagram in Fig. 4) , and the bottom nodes (i.e., nodes 1 and 2) are constrained using pinned/roller boundary conditions. The computational domain consists of two bilinear quadrilateral plane strain elements (CPE4), and a user defined zero thickness cohesive spring element at the interface. To establish the accuracy of the formulation, the difference between the computed values of the vertical displacements at the middle nodes (i.e., nodes 3, 4, 5, 6) and the corresponding theoretical values for the infinitely stiff case is evaluated. Our numerical results reported in Table II indicate that the proposed formulation guarantees stability and accuracy (close to machine precision) for large values of cohesive stiffness (i.e., for cohesive

Table I: SUMMARY OF MATERIAL PROPERTIES IN EACH NUMERICAL EXAMPLE

Material parameter (units)	E (N/mm^2)	v	G_{IC} (N/mm)	G_{IIC} (N/mm)	σ_{max} (N/mm^2)	τ_{max} (N/mm^2)
Patch test	1.00E+05	0.35	0.28	-	5.7	-
Mode I	1.00E+05	0.35	0.28	-	5.7	-
Mode II	1.00E+05	0.35	-	4	-	57
Mixed mode	1.00E+05	0.35	4	4	57	57

Table II: ACCURACY OF THE FORMULATION FOR THE UNIAXIAL TENSION TEST

Cohesive Stiffness (α_n) (N/mm)	% Error
1.00E+03	96.61
1.00E+05	22.17
1.00E+08	2.84E-02
1.00E+12	2.85E-06
1.00E+15	2.85E-09
1.00E+20	1.39E-14
1.00E+100	9.71E-14

stiffness up to 10^{100} N/mm). As expected the error between the computed and theoretical values decreases with an increase in the cohesive stiffness.
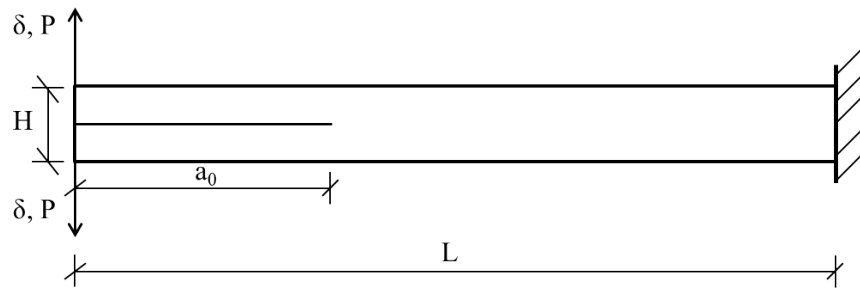
Mode I: Double Cantilever Beam (DCB) Test

Figure 5: Geometry and boundary conditions for the mode I double cantilever beam (DCB) test. The dimensions are: L = 100 mm, H = 4 mm and a_0 = 25 mm

Fig. 5 shows the set up of the double cantilever beam test. Fixed boundary condition is applied at the right end of the beam. A displacement is applied at the upper and lower nodes at the left end to initiate mode I delamination and the corresponding load is recorded. The simulation

is displacement controlled so as to capture the softening portion of the load-displacement curve. The computational mesh consists of bilinear quadrilateral elements (CPE4) and user-defined zero thickness cohesive elements. The load vs upper left node displacement curves for the isotropic material from the traditional CZM approach, proposed stabilized approach, and the analytical LEFM solution ([24]) are shown in Fig. 6. It can be seen in Fig. 6 that:

1. In traditional cohesive zone formulations, if the initial cohesive stiffness is very high, traction oscillations are commonly observed as a result of numerical instability in the formulation.

2. The proposed formulation alleviates numerical instability, consequently, the post-peak load-displacement curve is free of oscillations for any choice of initial cohesive stiffness.

3. The initial portion of the load-displacement curve obtained from proposed method shows an excellent match with the analytical curve.

4. The peak load obtained from the numerical simulation approaches the analytical (i.e., LEFM) peak load value as the cohesive strength is increased.

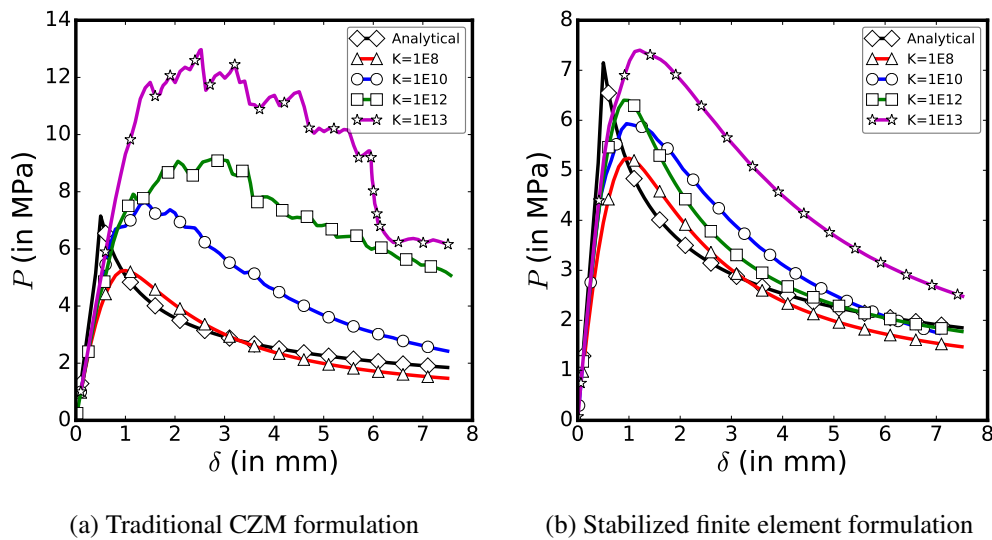(a) Traditional CZM formulation   (b) Stabilized finite element formulation

Figure 6: Load vs. displacement curves for an isotropic material from the mode-I delamination: (a) traditional CZM formulation shows instability for large stiffness values; (b) the stabilized formulation alleviates instabilities for large stiffness values.

Mixed Mode: Mixed Mode Bending (MMB) Test

The MMB test setup is shown in Fig. 7 (proposed by [25] as an alternative to the original configuration proposed in [26]). The beam of length 2L is simply supported at the lower left and right end

nodes. The forces applied on the upper and lower arm are obtained from superposition of mode I and mode II are given as:

$$P_u = P\frac{c+L}{4L} + P\frac{3c-L}{4L}, \tag{32}$$

$$P_d = P\frac{c+L}{4L} - P\frac{3c-L}{4L}, \tag{33}$$

where c is the length parameter that decides the ratio between the two forces, and thus defines the mixed mode ratio. The computational mesh for the beam is similar to that used for mode I. The load (P_u) vs displacement (δ) curves for the isotropic material from the traditional CZM, proposed stabilized method and the analytical LEFM solution [24] are shown in Fig. 8. Displacement control is used for the simulation in this case as well. The results reaffirm the applicability of the proposed stabilized approach.
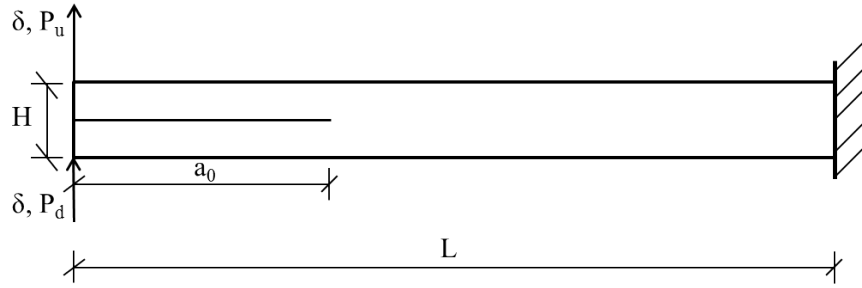

Figure 7: Geometry and boundary conditions for the mixed mode bending (MMB) test. The dimensions are: L = 100 mm, H = 4 mm and a_0 = 25 mm

Conclusion

In this work, we propose a unified formulation based on the Nitsche method that is equally effective for any specified stiffness of a cohesive law. We showed that when the cohesive stiffness approaches zero, the formulation collapses to a traditional finite element formulation with the cohesive law enforced as a Neumann boundary condition; on the other hand, as the stiffness approaches a large value, the proposed approach becomes identical to that of a standard Nitsche method and the cohesive law is enforced as a kinematic constraint. Thus, the key advantage is that it generalizes the Nitsche approach to a traction-separation law of any arbitrary initial stiffness and provides a unified way to treat such problems in a variationally consistent and stable manner. The stabilized finite element formulation would naturally extend to general nonlinear forms of traction-separation relationships, although we only use the bilinear cohesive law. We performed several numerical studies to demonstrate the advantages of the proposed approach over the standard CZM approach through

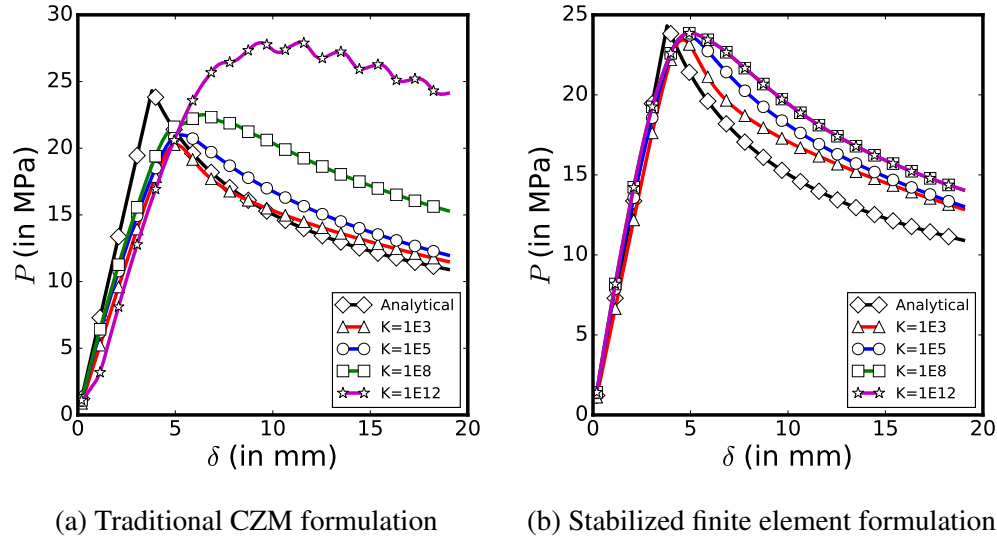(a) Traditional CZM formulation   (b) Stabilized finite element formulation

Figure 8: Load vs. displacement curves for the mixed mode bending test. Similar to the results of mode-I test, traditional CZM approach shows instability for large stiffness but the proposed stabilized approach is free of that

two benchmark problems: mode-I and mixed-mode delamination tests. The load-displacement curves obtained from these tests for traditional CZM formulation show instability and oscillation for large stiffness values, whereas, the stabilized formulation results are free of any numerical instabilities or oscillations. Moreover, results obtained from the stabilized formulation show much better agreement with the analytical solution in comparison to the traditional CZM formulation. Currently, the formulation is only implemented assuming linear isotropic elastic behavior in the bulk material domain and our future work will focus on extending the proposed method to model static delamination in transversely isotropic laminated composites. Another direction of future work is to model high cycle fatigue delamination of composites.

Acknowledgements

References

[1] D.S. Dugdale. Yielding of steel sheets containing slits. *Journal of the Mechanics and Physics of Solids*, 8(2):100–104, 1960.

[2] G.I. Barenblatt. The mathematical theory of equilibrium cracks in brittle fracture. *Advances in Applied Mechanics*, 7:55–129, 1962.

[3] G.H. Paulino, Z. Zhangb, and W. Celesc. Dynamic failure branching and fragmentation using coesive zone modeling. In *Convegno IGF XVIII Cetraro 2006*, 2008.

[4] V.P. Nguyen. Discontinuous Galerkin/extrinsic cohesive zone modeling: Implementation caveats and applications in computational fracture mechanics. *Engineering Fracture Mechanics*, 128:37–68, 2014.

[5] K. Park, G.H. Paulino, W. Celes, and R. Espinha. Adaptive mesh refinement and coarsening for cohesive zone modeling of dynamic fracture. *International Journal for Numerical Methods in Engineering*, 92(1):1–35, 2012.

[6] R. Espinha, K. Park, G.H. Paulino, and W. Celes. Scalable parallel dynamic fracture simulation using an extrinsic cohesive zone model. *Computer Methods in Applied Mechanics and Engineering*, 266:144–161, 2013.

[7] N. Blal, L. Daridon, Y. Monerie, and S. Pagano. Artificial compliance inherent to the intrinsic cohesive zone models: criteria and application to planar meshes. *International Journal of Fracture*, 178(1-2):71–83, 2012.

[8] P.D. Zavattieri and H.D. Espinosa. Grain level analysis of crack initiation and propagation in brittle materials. *Acta Materialia*, 49(20):4291–4311, 2001.

[9] J. Mergheim, E. Kuhl, and P. Steinmann. A hybrid discontinuous Galerkin/interface method for the computational modelling of failure. *International Journal for Numerical Methods in Biomedical Engineering*, 20(7):511–519, 2004.

[10] T.J. Truster and A. Masud. A discontinuous/continuous Galerkin method for modeling of interphase damage in fibrous composite systems. *Computational Mechanics*, 52(3):499–514, 2013.

[11] E. Lorentz. A mixed interface finite element for cohesive zone models. *Computer Methods in Applied Mechanics and Engineering*, 198(2):302–317, 2008.

[12] H. Ji and J.E. Dolbow. On strategies for enforcing interfacial constraints and evaluating jump conditions with the extended finite element method. *International Journal for Numerical Methods in Engineering*, 61(14):2508–2535, 2004.

[13] J. Nitsche. Über ein Variationsprinzip zur Lösung von Dirichlet-Problemen bei Verwendung von Teilräumen, die keinen Randbedingungen unterworfen sind. In *Abhandlungen aus dem mathematischen Seminar der Universität Hamburg*, volume 36, pages 9–15. Springer, 1971.

[14] I. Babuška. *Numerical solution of boundary value problems by the perturbed variational principle*. Institute for Fluid Dynamics and Appl. Math., Technical Note BN-624, University of Maryland, College Park, Md., 1969.

[15] F. Liu and R.I. Borja. A contact algorithm for frictional crack propagation with the extended finite element method. *International Journal for Numerical Methods in Engineering*, 76(10):1489–1512, 2008.

[16] P. Wriggers and G. Zavarise. A formulation for frictionless contact problems using a weak form introduced by Nitsche. *Computational Mechanics*, 41(3):407–420, 2008.

[17] A. Hansbo and P. Hansbo. An unfitted finite element method, based on Nitsches method, for elliptic interface problems. *Computer Methods in Applied Mechanics and Engineering*, 191(47):5537–5552, 2002.

[18] C. Annavarapu, M. Hautefeuille, and J.E. Dolbow. A robust Nitsche's formulation for interface problems. *Computer Methods in Applied Mechanics and Engineering*, 225:44–54, 2012.

[19] P. Hansbo. Nitsche's method for interface problems in computational mechanics. *GAMM-Mitteilungen*, 28(2):183–206, 2005.

[20] X. Liu, R. Duddu, and H. Waisman. Delamination analysis of composites using a finite element based discrete damage zone model. *Conference Proceedings, Society for the Advancement of Materials and Process Engineering (SAMPE), Baltimore, MD*, pages 1–15, 2012.

[21] X. Liu, R. Duddu, and H. Waisman. Discrete damage zone model for fracture initiation and propagation. *Engineering Fracture Mechanics*, 92:1–18, 2012.

[22] Stephen Jimenez, Xia Liu, Ravindra Duddu, and Haim Waisman. A discrete damage zone model for mixed-mode delamination of composites under high-cycle fatigue. *International Journal of Fracture*, 190(1-2):53–74, 2014.

[23] S. Jiménez and R. Duddu. On the parametric sensitivity of cohesive zone models for high-cycle fatigue delamination of composites. *International Journal of Solids and Structures*, 82:111–124, 2016.

[24] Y. Mi, M.A. Crisfield, G.A.O. Davies, and H.B. Hellweg. Progressive delamination using interface elements. *Journal of Composite Materials*, 32(14):1246–1272, 1998.

[25] S. Jiménez, X. Liu, R. Duddu, and H. Waisman. A discrete damage zone model for mixed-mode delamination of composites under high-cycle fatigue. *International Journal of Fracture*, 190(1-2):53–74, 2014.

[26] J.R. Reeder and J.H. Crews. Mixed-mode bending method for delamination testing. *AIAA Journal*, 28(7):1270–1276, 1990.